THE JOURNAL OF PHYSICAL CHEMISTRY C
A JOURNAL OF THE AMERICAN CHEMICAL SOCIETY

pubs.acs.org/JPCC

Article

X-ray Absorption Spectroscopic Study of the Transition-Metal-Only Double Perovskite Oxide Mn_2CoReO_6

Xiao Wang,* Jie Zhang, Zhao Pan, Dabiao Lu, Maocai Pi, Xubin Ye, Cheng Dong, Jie Chen, Kai Chen, Florin Radu, Sonia Francoual, Stefano Agrestini, Zhiwei Hu, Chun-Fu Chang, Arata Tanaka, Kazunari Yamaura, Yao Shen,* and Youwen Long*

Cite This: *J. Phys. Chem. C* 2024, 128, 15668−15675

Read Online

ACCESS | Metrics & More | Article Recommendations | Supporting Information

ABSTRACT: By means of X-ray absorption spectroscopic studies, both experimentally and theoretically, we investigated the magnetic properties of the transition-metal-only double perovskite oxide Mn_2CoReO_6, which experiences an antiferromagnetic transition at T_N = 93 K, whereas it holds a considerable net moment at low temperature. Internal exchange fields against the applied magnetic field for all the transition metal ions were identified, providing a microscopic insight into the intrasite antiferromagnetic couplings. Nevertheless, parallelly oriented canted spins of the Mn, Co, and Re cations were observed. In particularly, the Mn and Co cations hold considerable canting moments, which can be ascribed to the competition between the ferromagnetic intersite and antiferromagnetic intrasite magnetic interactions. Moreover, a spin-valve-type magnetoresistance was observed below the T_N. The concurrence of the magnetoresistance effect and the antiferromagnetic semiconductive nature make Mn_2CoReO_6 a promising candidate for high-speed and energy-saving spintronics applications.

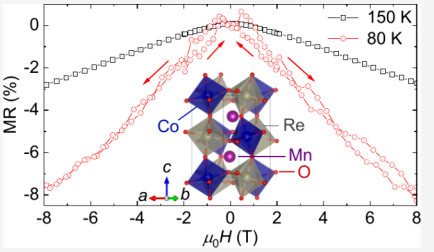

INTRODUCTION

The realization and utilization of both charge and spin degrees of freedom of the electrons underpin spintronics.[1−3] Reported spin-dependent electron transport mechanisms are giant magnetoresistance (GMR) in trilayer heterostructures with a nonmagnetic spacer sandwiched by two ferromagnetic (FM) electrodes,[4] tunnel magnetoresistance (TMR)[5] in magnetic tunnel junctions (MTJs), and magnetic random access memories (MRAMs).[6]

Antiferromagnetic (AFM) spintronics has attracted intense attention owing to its fast dynamics with frequency up to terahertz.[7] However, the zero net moment of the AFM materials severely impedes the manipulation of magnetization, leaving great challenges in applications. Nevertheless, multiple spin-dependent phenomena have been discovered in AFM materials that can encode and transport information through such as magnetoresistance (MR),[8] magnetoelectric multiferroics,[9] anomalous Hall effect,[10] spin torque,[11] magneto-optical Kerr effect,[12] etc. Therefore, AFM materials hold great opportunities for both academic studies and functional applications.

Double perovskite oxides with a formula of $A_2BB'O_6$ can flexibly accommodate different types of ions at the A, B, and B′ sites, making them attractive for engineering and studying potentially new spintronic materials. For example, the up-spin channel of Sr_2FeMoO_6 opens up a gap, while the down-spin channel is conductive, making it a half metal with 100% spin polarization and exhibiting GMR.[13,14] Similar half metallic behavior combined with GMR is also observed in double perovskite Sr_2FeReO_6.[15] Sr_2CrOsO_6 has a super high T_C of 725 K as a result of the robust AFM coupling between the Cr and Os ions at the B and B′ sites, respectively.[16] Y_2NiIrO_6 exhibits giant exchange bias attributable to the pinned magnetic domains due to the combination of strong spin−orbit coupling of the Ir ions and the AFM coupling of the Ni and Ir sublattices.[17] In most cases, the A site of double perovskites hosts nonmagnetic ions such as alkali, alkali earth, and lanthanides. Recent studies have shown that transition metals can also occupy the A site, resulting in novel magnetic and electronic interactions through the A-B and A-B′ pathways, further leading to intriguing properties for the transition-metal-only double perovskite oxides such as half metallicity,[18] GMR,[19] cation rattling,[20] and multiferroicity.[21]

Nevertheless, studies on transition-metal-only double perovskite oxides are still limited. The small transition metal at the A site leads to a significant mismatch between the A and B sites, resulting in significant tilt of the BO_6 octahedra. To the best of our knowledge, the few-reported transition-metal-only double perovskite oxides are prepared under high pressure over 5 GPa.[18−23] Mn_2CoReO_6 (MCRO) is the fourth known transition-metal-only double perovskite oxide.[23] It experiences

Received: July 5, 2024
Revised: September 3, 2024
Accepted: September 4, 2024
Published: September 10, 2024

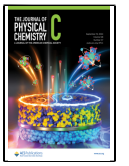

https://doi.org/10.1021/acs.jpcc.4c04491
J. Phys. Chem. C 2024, 128, 15668−15675

an antiferromagnetic transition at T_N = 93 K but possesses a considerable net moment at low temperature. In this paper, by experimental and theoretic X-ray absorption spectroscopic studies, we obtained a negative internal magnetic field for all the three transition metal cations, indicating the dominant AFM intrasite magnetic couplings. However, parallel canting spins of Mn, Co, and Re are identified. In particularly, the Mn and Co cations hold considerable canting moments, which can be ascribed to the competition between the intra- and intersites magnetic interactions between them. Moreover, a spin-valve-type MR effect was observed below T_N. Therefore, the MCRO holds basic traits that are relevant to future high-speed and energy-saving AFM spintronics applications.

METHODS

Polycrystalline MCRO was synthesized under high-pressure and high-temperature (HPHT) conditions. Stoichiometric high-purity (>99.9%) starting materials MnO, CoO, and ReO_3 were thoroughly ground with an agate mortar in an argon gas atmosphere. Then, the mixed powder was pressed into a platinum capsule of 3 mm diameter and 4 mm height and then treated with an anvil-type high-pressure apparatus under 9 GPa and 1523 K for 30 min. After the HPHT treatment, the temperature was quenched to room temperature in seconds, and the pressure was slowly released to ambient in several hours.

The synchrotron X-ray diffraction (SXRD) patterns were collected at the BL02B2 (λ = 0.65 Å) beamline of SPring-8 in Hyogo. The 2θ scan was performed from 2 to 70° with a step of 0.006°. The Rietveld refinement of crystallographic parameters was performed using the GSAS software package.[24] The magnetic susceptibility and magnetization were measured by using a Quantum Design superconducting quantum interference device magnetometer (MPMS-3). Both zero-field-cooling (ZFC) and field-cooling (FC) modes were adopted for magnetic susceptibility measurements with a 0.1 T magnetic field. The electrical resistivity was measured using a sample pellet with the size of about 2 × 1 × 1 mm^3 by a standard four-probe method on a Quantum Design physical property measurement system (PPMS-7). The heat capacity was measured using a sample pellet of a size of about 2 × 2 × 0.4 mm^3 on PPMS-7.

The Mn-$L_{2,3}$ and Co-$L_{2,3}$ X-ray absorption spectra (XAS) were measured at room temperature via total electron yield (TEY) mode at the TPS 45A beamline of National Synchrotron Radiation Research Center (NSRRC) in Hsinchu. The Mn-$L_{2,3}$ and Co-$L_{2,3}$ X-ray magnetic circular dichroism (XMCD) spectra were measured at 10 K and 8 T using TEY mode at the VEKMAG end station[25] at the HZB/BESSY II synchrotron radiation facility in Berlin. The XAS and XMCD at the Re-$L_{2,3}$ edges were measured in transmission at beamline P09 at PETRA III at DESY in Hamburg, and the Re-$L_{2,3}$ XMCD was measured at 10 K and 5 T. For the XMCD measurements, both the magnetic field and polarization (~77% for VEKMAG and ~99% for P09) of the light were flipped to obtain the μ^+ (parallel) and μ^- (antiparallel) spectra.

RESULTS AND DISCUSSION

Figure 1 displays the SXRD pattern of MCRO, which can be refined with the space group $P2_1/n$ (no. 14) with lattice parameters of a = 5.23506(1) Å, b = 5.35179(1) Å, c = 7.63109(2) Å, and β = 89.966(0)°. The crystal structure was depicted in the inset at the right side of Figure 1. As shown in Figure 1 and the inset in the middle, the (011) diffraction peak clearly indicates the rocksalt-type distribution of Co and Re at the B and B′ sites, respectively.[26] A slight antisite occupancy of 2% between Co and Re was found. A previous neutron powder diffraction (NPD) also indicated ~16% disorder between A-site Mn and B-site Co.[23] The detailed refined parameters from SXRD are given in Table S1. The valence states of Mn^{2+} and Co^{2+} can be obtained via the bond valence sum (BVS)[27] calculations based on the refined bond lengths (Table S2). For Re, the averaged Re−O bond length is 1.920 Å, very close to that of $Sr_2MgRe^{6+}O_6$ (1.912 Å),[28] indicating a Re^{6+} state for MCRO.

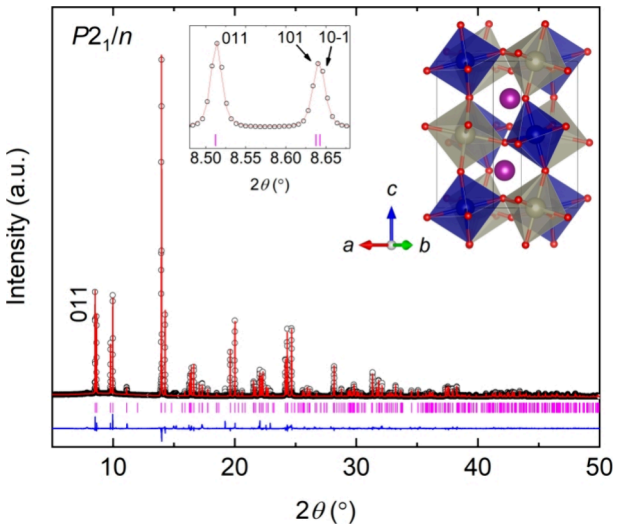

Figure 1. SXRD pattern and Rietveld refinement of MCRO. The black circles, red lines, and blue lines indicate the observed, calculated, and difference, respectively. The magenta ticks indicate the allowed Bragg reflections for the space group $P2_1/n$. The inset in the middle displays the SXRD pattern near the (011) diffraction peaks. The inset at the right side displays the crystal structure of MCRO. Mn, Co, Re, and O are shown in purple, blue, gray, and red, respectively.

To directly obtain the valence states of the cations in MCRO, we performed XAS measurements. It is well-known that XAS is an element-selective technique highly sensitive to the valence state. For an open d shell system, an increase in the valence of the transition metal ion by one leads to a shift of the $L_{2,3}$ XAS spectrum to higher energies by one electronvolt (eV) or more that is also accompanied by remarkable changes of the spectral feature.[29−31] As shown in Figure 2a, the white line of the Mn-$L_{2,3}$ XAS of MCRO resembles that of Mn^{2+} reference compound MnO with the L_2/L_3 peak locating at the same energy as that of MnO, which points to the occurrence of a Mn^{2+} valence state. Similarly, as shown in Figure 2b and Figure 2c, the peak energies and shape of the white lines of the Co-$L_{2,3}$ and Re-L_3 XAS respectively resemble those of the high-spin Co^{2+} and Re^{6+} references,[32] indicating the occurrence of high-spin Co^{2+} ($t_{2g}^5e_g^2$) and Re^{6+} valence states. Therefore, the valence configuration $Mn^{2+}/Co^{2+}/Re^{6+}$ is experimentally validated.

After the determination of the structure and valence states, we continue with the description of the magnetic properties of MCRO. Figure 3a displays the temperature-dependent magnetic susceptibility of MCRO. At T_N = 93 K, an AFM transition can be clearly identified. An NPD study has demonstrated that this AFM transition is related to the

https://doi.org/10.1021/acs.jpcc.4c04491
J. Phys. Chem. C 2024, 128, 15668−15675

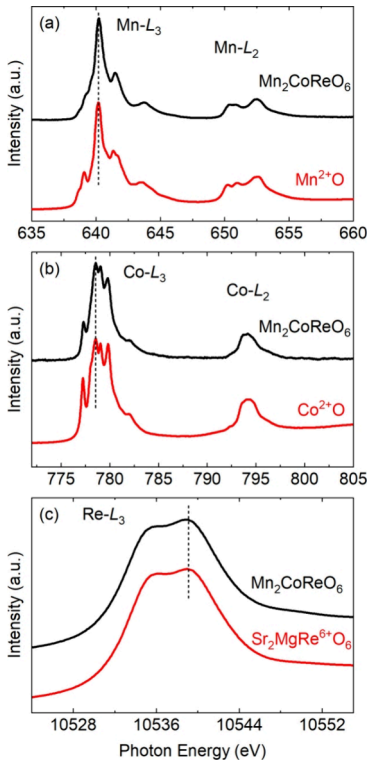

Figure 2. XAS at the (a) Mn-$L_{2,3}$, (b) Co-$L_{2,3}$, and (c) Re-L_3 edges of MCRO. The XAS of MnO, CoO, and Sr_2MgReO_6 are displayed as Mn^{2+}, Co^{2+}, and Re^{6+} references, respectively.

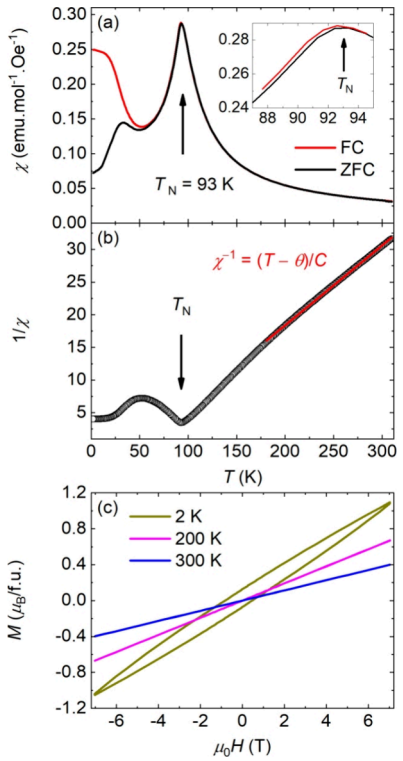

Figure 3. (a) Temperature-dependent magnetic susceptibility of MCRO. The inset displays the region near T_N = 93 K. (b) The inversed magnetic susceptibility (black circles) and the Curie−Weiss fitting above 180 K with the formula $\chi^{-1} = (T - \theta)/C$. (c) Field-dependent magnetization of MCRO at selected temperatures.

antiparallel spin alignment of all of the Mn, Co, and Re sublattices.[23] It is worth noting that the AFM transition is relatively broad in temperature, as an implication of competing FM and AFM coupling mechanisms. Moreover, the ZFC and FC curves start to separate below T_N (see the inset of Figure 3a) and further split with the temperature decreasing, indicating the formation of a canted AFM structure. As shown in Figure 3b, the Curie−Weiss fitting was performed above 180 K with the function $\chi^{-1} = (T - \theta)/C$. The positive Weiss temperature θ = 50 K indicates the presence of FM interactions in Mn_2CoReO_6. According to the fitted Curie constant, C = 8.18 emu K mol^{-1} Oe^{1-}, the effective magnetic moment is calculated to be μ_{exp} = 8.09 $(\sqrt{8C})$ Bohr magnetons per formula unit (μ_B/f.u.), slightly smaller than the spin-only theoretical value of 9.38 μ_B/f.u. $(g\sqrt{\sum_i S_i(S_i + 1)}$, where g = 2 is the Landé factor of spins), considering Mn^{2+} (S = 5/2), Co^{2+} (S = 3/2, high spin), and Re^{6+} (S = 1/2) ions. The smaller experimental value can be a result of a reduction of the Re^{6+} moment through the spin−orbit coupling. Figure 3c displays the isothermal field-dependent magnetization of the MCRO. At temperatures above T_N, the magnetization is linearly dependent on the magnetic field, in agreement with a paramagnetic state. When the temperature further decreases down to 2 K, a prominent hysteresis and moment of 1.1 μ_B/f.u. at 7 T can be found, which is indicative of the competition between the AFM and FM couplings, which will be discussed later.

We further measured the heat capacity of the MCRO. As shown in Figure 4a, a cusp feature emerges at T_N, in agreement

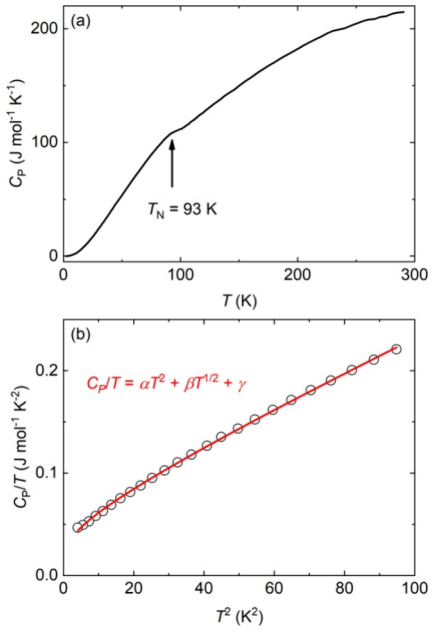

Figure 4. (a) Temperature-dependent heat capacity of MCRO. (b) Experimental heat capacity below 10 K (black circles) and the fitting with the formula $C_P/T = \alpha T^2 + \beta T^{1/2} + \gamma$ (red line).

with the AFM transition. It is worth noting that this feature is relatively weak, quite different from the sharp peak expected at AFM transitions.[33] To display the ingredients that contribute to the heat capacity, we plotted the C_P/T-T^2 plot below 10 K, as depicted in Figure 4b. The convex curve at low temperature clearly indicates the magnetic contribution on the specific heat,

https://doi.org/10.1021/acs.jpcc.4c04491
J. Phys. Chem. C 2024, 128, 15668−15675

in accord with the concurrence of both magnetic and antiferromagnet interactions in MCRO. The heat capacity can be well fitted with formula $C_p/T = \alpha T^2 + \beta T^{1/2} + \gamma$, with α = 1.53 mJ mol^{-1} K^{-4}, β = 23.5 mJ mol^{-1} K$^{-5/2}$, and γ = 4.24 mJ mol^{-1} K^{-2}, indicating that the phonons, magnons, and electrons all contribute to the heat capacity, in agreement with the canted AFM semiconductive nature of MCRO.

To obtain a deeper insight into the configuration of the canted spins, we performed XMCD measurements on the Mn, Co, and Re ions. It is known that the element-selective XMCD is a sensitive probe for determining the spin alignment of the magnetic ions.[32,34,35] As shown in Figure 5, the XMCD signal

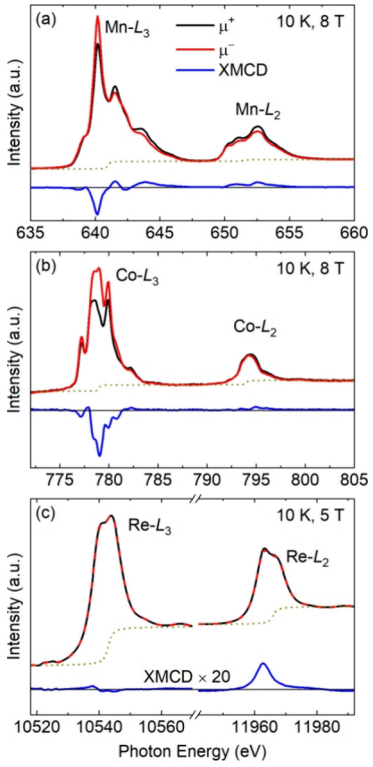

Figure 5. XMCD spectra at the (a) Mn-$L_{2,3}$, (b) Co-$L_{2,3}$, and (c) Re-$L_{2,3}$ edges of MCRO. XAS with light polarization parallel (μ^+, black lines) and antiparallel (μ^-, red lines) to the magnetic field are shown. The blue lines are the XMCD ($\mu^+ - \mu^-$) spectra. The dashed lines indicate an edge jump.

at the L_3 (L_2) edge of all transition metals is negative (positive), demonstrating that the resultant spins direction of Mn, Co, and Re are parallel to each other in an applied magnetic field.[36,37] Herein, MCRO provides a very rare example of double perovskites with parallel spins at all A, B, and B′ sites. Usually, the superexchange interaction between the 5d and 3d ions through the A/B−O−B′ pathway and the two sublattice double-exchange mechanism[38] play roles on the magnetic property. For example, in Sr_2FeReO_6, Sr_2CrOsO_6, and Y_2NiIrO_6, the B-site 3d and B′-site 5d ions are ferrimagnetically (FiM) coupled.[15−17] Similar FiM structures can be also found in the quadruple perovskite oxides $CaCu_3Fe_2B'_2O_{12}$ (B′ = Re and Os).[39−41]

One can observe that the XMCD signals for all the three cations Mn, Co, and Re are much smaller than the typical ferromagnets,[42,43] as the net magnetization is from canted spins. To obtain an inner view of the magnetic moments of the cations, we performed full-atomic-multiplet ligand-field calculations using the XTLS code.[44] This theoretical calculation includes the full intra-atomic multiplet interactions, the atomic d spin−orbit coupling (SOC), the transition metal d to O-2p hybridization, and the crystal field interaction. This model has very successfully reproduced the line shape of XMCD spectra of transition metal elements in the past decades.[45,46] The parameters are listed in ref 47. The calculations reproduce the measured spectra well, as shown in Figure 6. In our

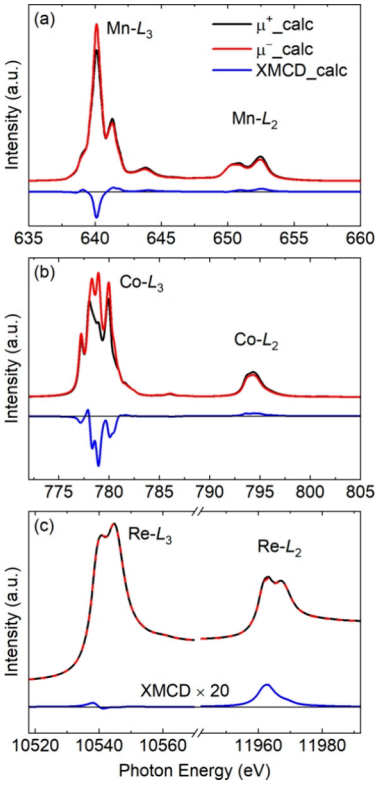

Figure 6. Calculated XMCD spectra at the (a) Mn-$L_{2,3}$, (b) Co-$L_{2,3}$, and (c) Re-$L_{2,3}$ edges of MCRO. The XAS with light polarization parallel (μ^+, black lines) and antiparallel (μ^-, red lines) to the magnetic field are shown. The blue lines are the XMCD ($\mu^+ - \mu^-$) spectra.

calculations, to obtain the intensity of the XMCD signal, negative exchange fields (H_{ex}) were adopted for all the three transition metal ions Mn^{2+}, Co^{2+}, and Re^{6+}.[47] The negative H_{ex} is indicative of an internal magnetic field against the applied field. These results provide a microscopic insight of the intrasite AFM couplings of the Mn, Co, and Re sublattices.

From the cluster calculations, the spin and orbital moments of Mn, Co, and Re are listed in Table 1, leading to a total moment of 1.83 μ_B/f.u. The obtained total moment larger than that for the magnetization measurements (Figure 3c) could be a result of the stronger applied magnetic field for the XMCD

Table 1. Spin and Orbital Moments Obtained from the Cluster Calculations

cation	M_{spin} (μ_B/atom)	M_{orb} (μ_B/atom)
Mn	0.471	
Co	0.638	0.251
Re	0.0159	−0.0144

https://doi.org/10.1021/acs.jpcc.4c04491
J. Phys. Chem. C 2024, 128, 15668−15675

measurements. One can also find considerable spin moments of Mn and Co, indicating that the spins of Mn and Co are notably canted along the applied magnetic field. Note that the orbital moment of Mn^{2+} is negligible because of the half-filled 3*d* orbit ($t_{2g}^{3}\uparrow e_g^{2}\uparrow$). On the contrary, the spin moment of Re is very small, indicating that the collinear AFM alignment of the Re spins is almost maintain.

To understand the different canting behavior between Mn/Co and Re sites, we discuss the possible magnetic interactions in MCRO. The intrasite AFM structure is indicative of the dominate long-range superexchange pathway M-O-M′-O-M, as a consequence of the energy differences of the orbitals between the M and M′ ions.[48,49] Here, in MCRO, different orbitals of 3*d*-e_g, 3*d*-t_{2g}, and 5*d*-t_{2g} for Mn^{2+} ($3d^5$), Co^{2+} ($3d^7$), and Re^{6+} ($5d^1$), respectively, are involved in the magnetic couplings, giving rise of the domination of the long-range superexchange couplings. On the other hand, the canted moments of MCRO indicate the competition of magnetic interactions against the long-range superexchange one. Here, we consider the super-expande pathway M-O-M′. As shown in Figure 7 and Table S3,

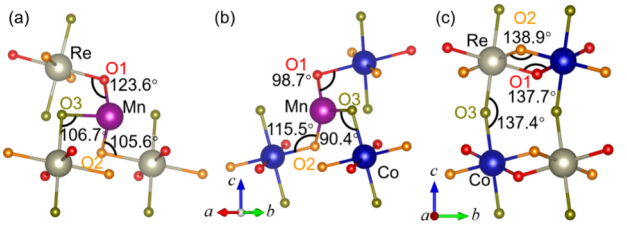

Figure 7. Bond angles of (a) Mn−O−Re, (b) Mn−O−Co, and (c) Co−O−Re. The Mn, Co, and Re ions are shown in purple, blue, and gray, respectively. The different O sites are shown in red, orange, and brown, respectively.

the bond angle(s) ∠Mn−O−Co and ∠Mn−O−Re are close to 90°, and ∠Co−O−Re is close to 180°. According to the Goodenough−Kanamori−Anderson rules,[50−52] the B-site Co is FM coupled with both the A-site Mn and B′-site Re ions, and Mn and Re are AFM coupled. On account of the localized 3*d* orbit, the FM intersite superexcharge interaction between Mn and Co is supposed to play a role, thus competing with the AFM intrasite couplings. It therefore explains that Co and Mn hold considerable canted spins, whereas the spin of Re almost maintains the antiparallel alignment as listed in Table 1.

We further investigated the transport properties of MCRO. As shown in Figure 8a, the electrical resistivity increases with cooling, exceeding the measuring range (10^6 Ω cm) below 80 K, indicating either semiconductive or insulative behavior. The temperature-dependent electrical resistivity can be well fitted with the thermal activation model within the temperature range 260−350 K with the formula $\rho = \rho_0 \times \exp(E_a/k_BT)$, where ρ_0 and E_a represent the residual resistance and activation energy, respectively, and k_B is the Boltzmann constant. This demonstrates that the MCRO is a semiconductor. The obtained energy gap from the fitting is $E_k = 2E_a = 0.29$ eV, and the residual resistance is 0.11 Ω cm.

The canted AFM structure with a considerable net magnetic moment allows MCRO to be utilized as high-speed spin filtering by means of the TMR mechanism through magnetic domains and grain boundaries of polycrystalline MCRO.[5,14] As displayed in Figure 8b, at 150 K ($>T_N$), the MR of MCRO is almost independent of the magnetic field, in agreement with a paramagnetic state. Note that the slight decrease in MR is

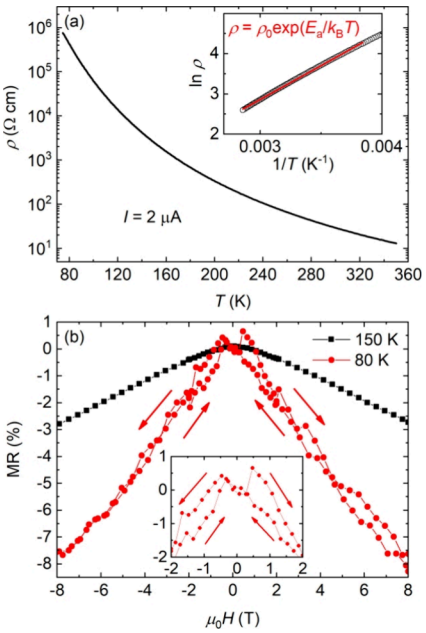

Figure 8. (a) Temperature-dependent electrical resistivity of MCRO. The inset displays the experimental data (black circles) and the thermal activation model fitting with formula $\rho = \rho_0 \times \exp(E_a/k_BT)$ in the temperature range 260−350 K. (b) Field-dependent magnetoresistances of MCRO at 150 and 80 K. The inset depicts the region of ±2 T.

caused by some extrinsic effects such as short-range magnetic correlations. On the other hand, at 80 K ($<T_N$), the MR increases to positive values under small magnetic field and then decreases to negative values upon further magnetic field increase and is accompanied by a prominent coercivity. This butterfly-shaped MR is reminiscent of the spin-valve-type transport mechanism, which is in accordance with the tunnel effect between multilayer junctions and/or grain boundaries.[13,14,53,54] The MR reaches 8% at 80 K and 7 T and depends linearly on the applied magnetic field above 2 T. Note that the electrical resistivity exceeds the measuring range below 80 K. To take into consideration of the large coercivity at 2 K which can lead to a strong pining effect of the spins,[17] we thus speculate a much larger MR at lower temperatures for a more conductive MCRO sample through disordering, doping, and/or oxygen vacancies.

CONCLUSIONS

In summary, the transition-metal-only double perovskite oxide Mn_2CoReO_6 was studied by element-selective X-ray absorption spectroscopy. The valence states of $Mn^{2+}/Co^{2+}/Re^{6+}$ were experimentally determined. An internal magnetic field against with the applied magnetic field was obtained, providing a microscopic insight of the intrasite antiferromagnetic couplings. Nevertheless, X-ray magnetic circular dichroic measurements manifest that all the Mn, Co, and Re spins are canted and parallel with each other, and particularly, the 3*d* Mn and Co cations hold considerable canting moments, which can be ascribed to the competition between the intra- and intersites magnetic interactions. Moreover, a spin-valve-type magnetoresistance was observed below T_N, which results from the spin-valve-type tunneling through the grain boundaries. The concurrence of the antiferromagnetic nature and the magneto-

https://doi.org/10.1021/acs.jpcc.4c04491
J. Phys. Chem. C 2024, 128, 15668−15675

resistance effect makes Mn_2CoReO_6 a promising candidate for high-speed and energy-saving spintronics applications.

■ ASSOCIATED CONTENT

Supporting Information

The Supporting Information is available free of charge at https://pubs.acs.org/doi/10.1021/acs.jpcc.4c04491.

Detailed lattice parameters, bond lengths, and bond angles from SXRD refinement (PDF)

■ AUTHOR INFORMATION

Corresponding Authors

Xiao Wang − *Beijing National Laboratory for Condensed Matter Physics, Institute of Physics, Chinese Academy of Sciences, Beijing 100190, China;* orcid.org/0000-0001-8139-4192; Email: wangxiao@iphy.ac.cn

Yao Shen − *Beijing National Laboratory for Condensed Matter Physics, Institute of Physics, Chinese Academy of Sciences, Beijing 100190, China; School of Physical Sciences, University of Chinese Academy of Sciences, Beijing 100049, China*; Email: yshen@iphy.ac.cn

Youwen Long − *Beijing National Laboratory for Condensed Matter Physics, Institute of Physics, Chinese Academy of Sciences, Beijing 100190, China; School of Physical Sciences, University of Chinese Academy of Sciences, Beijing 100049, China; Songshan Lake Materials Laboratory, Dongguan, Guangdong 523808, China;* orcid.org/0000-0002-8587-7818; Email: ywlong@iphy.ac.cn

Authors

Jie Zhang − *Beijing National Laboratory for Condensed Matter Physics, Institute of Physics, Chinese Academy of Sciences, Beijing 100190, China; School of Physical Sciences, University of Chinese Academy of Sciences, Beijing 100049, China;* orcid.org/0009-0006-9055-2969

Zhao Pan − *Beijing National Laboratory for Condensed Matter Physics, Institute of Physics, Chinese Academy of Sciences, Beijing 100190, China;* orcid.org/0000-0002-8693-2508

Dabiao Lu − *Beijing National Laboratory for Condensed Matter Physics, Institute of Physics, Chinese Academy of Sciences, Beijing 100190, China; School of Physical Sciences, University of Chinese Academy of Sciences, Beijing 100049, China;* orcid.org/0009-0006-5489-2835

Maocai Pi − *Beijing National Laboratory for Condensed Matter Physics, Institute of Physics, Chinese Academy of Sciences, Beijing 100190, China; School of Physical Sciences, University of Chinese Academy of Sciences, Beijing 100049, China*

Xubin Ye − *Beijing National Laboratory for Condensed Matter Physics, Institute of Physics, Chinese Academy of Sciences, Beijing 100190, China;* orcid.org/0000-0002-5739-8318

Cheng Dong − *Beijing National Laboratory for Condensed Matter Physics, Institute of Physics, Chinese Academy of Sciences, Beijing 100190, China*

Jie Chen − *Laboratory for Materials and Structures, Institute of Innovative Research, Tokyo Institute of Technology, Yokohama, Kanagawa 226-8503, Japan;* orcid.org/0000-0001-9609-669X

Kai Chen − *National Synchrotron Radiation Laboratory, University of Science and Technology of China, Hefei 230026, China*

Florin Radu − *Helmholtz-Zentrum Berlin fur Materialien und Energie, Berlin 12489, Germany*

Sonia Francoual − *Deutsches Elektronen-Synchrotron (DESY), Hamburg 22607, Germany*

Stefano Agrestini − *Diamond Light Source, Didcot OX11 0DE, United Kingdom;* orcid.org/0000-0002-3625-880X

Zhiwei Hu − *Max Planck Institute for Chemical Physics of Solids, Dresden 01187, Germany;* orcid.org/0000-0003-0324-2227

Chun-Fu Chang − *Max Planck Institute for Chemical Physics of Solids, Dresden 01187, Germany*

Arata Tanaka − *Quantum Matter Program, Graduate School of Advanced Science and Engineering, Hiroshima University, Higashi-hiroshima 739-8530, Japan*

Kazunari Yamaura − *Research Center for Materials Nanoarchitectonics (MANA), National Institute for Materials Science, Tsukuba, Ibaraki 305-0044, Japan; Graduate School of Chemical Sciences and Engineering, Hokkaido University, Sapporo, Hokkaido 060-0810, Japan;* orcid.org/0000-0003-0390-8244

Complete contact information is available at: https://pubs.acs.org/10.1021/acs.jpcc.4c04491

Notes

The authors declare no competing financial interest.

■ ACKNOWLEDGMENTS

This work was supported by the National Key R&D Program of China (grant no. 2021YFA1400300), the National Natural Science Foundation of China (grants nos. 11934017, 12261131499, 11921004, 12304159, and 12304268), the Beijing Natural Science Foundation (grant no. Z200007), and the Chinese Academy of Sciences (grant no. XDB33000000). The synchrotron x-ray diffraction experiments were performed at SPring-8 with the approval of the Japan Synchrotron Radiation Research Institute (2023B1575). The authors thank DESY (Hamburg, Germany), a member of the Helmholtz Association HGF, for the provision of experimental facilities. Parts of this research were carried out at beamline P09 at PETRA III under proposal I-20200812. The 6*T*/2T/2T used for the XMCD measurements at P09 was funded in part by the BMBF grant no. 05K2013 from the German Federal Ministry of Education and Research. The authors thank J. Linares Mardegan and Olaf Leupold for scientific and technical support at P09. Financial support for developing and building the PM2-VEKMAG beamline and VEKMAG end station was provided by HZB and BMBF (grant nos. 05K10PC2, 05K10WR1, and 05K10KE1). The research in Dresden was partially supported by the DFG through SFB 1143. The authors acknowledge the support from the Max Planck-POSTECH-Hsinchu Center for Complex Phase Materials.

■ REFERENCES

(1) Fert, A. Nobel lecture: origin, development, and future of spintronics. *Rev. Mod. Phys.* **2008**, *80*, 1517−1530.

(2) Bibes, M.; Villegas, J. E.; Barthélémy, A. Ultrathin oxide films and interfaces for electronics and spintronics. *Adv. Phys.* **2011**, *60*, 5−84.

(3) Fusil, S.; Garcia, V.; Barthélémy, A.; Bibes, M. Magnetoelectric devices for spintronics. *Annu. Rev. Mater. Res.* **2014**, *44*, 91−116.

(4) Baibich, M. N.; Broto, J. M.; Fert, A.; Van Dau, F. N.; Petroff, F.; Etienne, P.; Creuzet, G.; Friederich, A.; Chazelas, J. Giant magnetoresistance of (001)Fe/(001)Cr magnetic superlattices. *Phys. Rev. Lett.* **1988**, *61*, 2472−2475.
(5) Moodera, J. S.; Kinder, L. R.; Wong, T. M.; Meservey, R. Large magnetoresistance at room temperature in ferromagnetic thin film tunnel junctions. *Phys. Rev. Lett.* **1995**, *74*, 3273−3276.
(6) Bhatti, S.; Sbiaa, R.; Hirohata, A.; Ohno, H.; Fukami, S.; Piramanayagam, S. N. Spintronics based random access memory: a review. *Mater. Today* **2017**, *20*, 530−548.
(7) Kampfrath, T.; Sell, A.; Klatt, G.; Pashkin, A.; Mährlein, S.; Dekorsy, T.; Wolf, M.; Fiebig, M.; Leitenstorfer, A.; Huber, R. Coherent terahertz control of antiferromagnetic spin waves. *Nat. Photonics* **2011**, *5*, 31−34.
(8) Qin, P.; Yan, H.; Wang, X.; Chen, H.; Meng, Z.; Dong, J.; Zhu, M.; Cai, J.; Feng, Z.; Zhou, X.; et al. Room-temperature magnetoresistance in an all-antiferromagnetic tunnel junction. *Nature* **2023**, *613*, 485−489.
(9) Wang, X.; Chai, Y.; Zhou, L.; Cao, H.; Cruz, C.; Yang, J.; Dai, J.; Yin, Y.; Yuan, Z.; Zhang, S.; et al. Observation of magnetoelectric multiferroicity in a cubic perovskite system: $LaMn_3Cr_4O_{12}$. *Phys. Rev. Lett.* **2015**, *115*, No. 087601.
(10) Nakatsuji, S.; Kiyohara, N.; Higo, T. Large anomalous Hall effect in a non-collinear antiferromagnet at room temperature. *Nature* **2015**, *527*, 212−215.
(11) Železný, J.; Wadley, P.; Olejník, K.; Hoffmann, A.; Ohno, H. Spin transport and spin torque in antiferromagnetic devices. *Nat. Phys.* **2018**, *14*, 220−228.
(12) Němec, P.; Fiebig, M.; Kampfrath, T.; Kimel, A. V. Antiferromagnetic opto-spintronics. *Nat. Phys.* **2018**, *14*, 229−241.
(13) Kobayashi, K.-I.; Kimura, T.; Sawada, H.; Terakura, K.; Tokura, Y. Room-temperature magnetoresistance in an oxide material with an ordered double-perovskite structure. *Nature* **1998**, *395*, 677−680.
(14) Sarma, D. D.; Ray, S.; Tanaka, K.; Kobayashi, M.; Fujimori, A.; Sanyal, P.; Krishnamurthy, H. R.; Dasgupta, C. Intergranular magnetoresistance in Sr_2FeMoO_6 from a magnetic tunnel barrier mechanism across grain boundaries. *Phys. Rev. Lett.* **2007**, *98*, No. 157205.
(15) Kobayashi, K.-I.; Kimura, T.; Tomioka, Y.; Sawada, H.; Terakura, K.; Tokura, Y. Intergrain tunneling magnetoresistance in polycrystals of the ordered double perovskite Sr_2FeReO_6. *Phys. Rev. B* **1999**, *59*, 11159−11162.
(16) Chen, J.; Wang, X.; Hu, Z.; Tjeng, L. H.; Agrestini, S.; Valvidares, M.; Chen, K.; Nataf, L.; Baudelet, F.; Nagao, M.; et al. Enhanced magnetization of the highest-T_C ferrimagnetic oxide Sr_2CrOsO_6. *Phys. Rev. B* **2020**, *102*, No. 184418.
(17) Deng, Z.; Wang, X.; Wang, M.; Shen, F.; Zhang, J.; Chen, Y.; Feng, H. L.; Xu, J.; Peng, Y.; Li, W.; et al. Giant exchange-bias-like effect at low cooling fields induced by pinned magnetic domains in Y_2NiIrO_6 double perovskite. *Adv. Mater.* **2023**, *35*, No. 2209759.
(18) Li, M.-R.; Retuerto, M.; Deng, Z.; Stephens, P. W.; Croft, M.; Huang, Q.; Wu, H.; Deng, X.; Kotliar, G.; Sánchez-Benítez, J.; et al. Giant magnetoresistance in the half-metallic double-perovskite ferrimagnet Mn_2FeReO_6. *Angew. Chem., Int. Ed.* **2015**, *54*, 12069−12073.
(19) Arévalo-López, A. M.; McNally, G. M.; Attfield, J. P. Large magnetization and frustration switching of magnetoresistance in the double-perovskite ferrimagnet Mn_2FeReO_6. *Angew. Chem., Int. Ed.* **2015**, *54*, 12074−12077.
(20) Akizuki, Y.; Yamada, I.; Fujita, K.; Taga, K.; Kawakami, T.; Mizumaki, M.; Tanaka, K. Rattling in the quadruple perovskite $CuCu_3V_4O_{12}$. *Angew. Chem., Int. Ed.* **2015**, *54*, 10870−10874.
(21) Li, M.-R.; McCabe, E. E.; Stephens, P. W.; Croft, M.; Collins, L.; Kalinin, S. V.; Deng, Z.; Retuerto, M.; Gupta, A. S.; Padmanabhan, H.; et al. Magnetorestriction-polarization coupling in multiferroic Mn_2MnWO_6. *Nat. Commun.* **2017**, *8*, 2037.
(22) Li, M.-R.; Hodges, J. P.; Retuerto, M.; Deng, Z.; Stephens, P. W.; Croft, M. C.; Deng, X.; Kotliar, G.; Sánchez-Benítez, J.; Walker, D.; et al. Mn_2MnReO_6: Synthesis and magnetic structure determination of a new transition-metal-only double perovskite canted antiferromagnet. *Chem. Mater.* **2016**, *28*, 3148−3158.
(23) Frank, C. E.; McCabe, E. E.; Orlandi, F.; Manuel, P.; Tan, X.; Deng, Z.; Croft, M.; Cascos, V.; Emge, T.; Feng, H. L.; et al. Mn_2CoReO_6: a robust multisublattice antiferromagnetic perovskite with small A-site cations. *Chem. Commun.* **2019**, *55*, 3331−3334.
(24) Larson, C.; Von Dreele, R. B. *General structure analysis system (GSAS)*, Report No. LAUR 86−748 (Los Alamos National Laboratory: Los Alamos, NM, 1994).
(25) Noll, T.; Radu, F. *The mechanics of the VEKMAG experiment. Proceedings of the 9th mechanical engineering design of synchrotron radiation equipment and instrumentation conference (MEDSI2016)*, JACoW: Barcelona, Spain, 2016, 370−373.
(26) Retuerto, M.; García-Hernández, M.; Martínez-Lope, M. J.; Fernández-Díaz, M. T.; Attfield, J. P.; Alonso, J. A. Switching from ferro- to antiferromagnetism in A_2CrSbO_6 (A = Ca, Sr) double perovskites: a neutron diffraction study. *J. Mater. Chem.* **2007**, *17*, 3555−3561.
(27) Brown, I. D.; Altermatt, D. Bond-valence parameters obtained from a systematic analysis of the inorganic crystal structure database. *Acta Crystallogr.* **1985**, *41*, 244−247. B41,
(28) Wiebe, C. R.; Greedan, J. E.; Kyriakou, P. P.; Luke, G. M.; Gardner, J. S.; Fukaya, A.; Gat-Malureanu, I. M.; Russo, P. L.; Savici, A. T.; Uemura, Y. J. Frustration-driven spin freezing in the $S = 1/2$ fcc perovskite Sr_2MgReO_6. *Phys. Rev. B* **2003**, *68*, No. 134410.
(29) Burnus, T.; Hu, Z.; Wu, H.; Cezar, J. C.; Niitaka, S.; Takagi, H.; Chang, C.-F.; Brookes, N. B.; Lin, H.-J.; Jang, L.-Y.; et al. X-ray absorption and x-ray magnetic dichroism study on Ca_3CoRhO_6 and Ca_3FeRhO_6. *Phys. Rev. B* **2008**, *77*, No. 205111.
(30) Chen, J.-M.; Chin, Y.-Y.; Valldor, M.; Hu, Z.; Lee, J.-M.; Haw, S.-C.; Hiraoka, N.; Ishii, H.; Pao, C.-W.; Tsuei, K.-D.; et al. A complete high-to-low spin state transition of trivalent cobalt ion in octahedral symmetry in $SrCo_{0.5}Ru_{0.5}O_{3-\delta}$. *J. Am. Chem. Soc.* **2014**, *136*, 1514−1519.
(31) Hu, Z.; Golden, M. S.; Fink, J.; Kaindl, G.; Warda, S. A.; Reinen, D.; Mahadevan, P.; Sarma, D. D. Hole distribution between the Ni 3*d* and O 2*p* orbitals in $Nd_{2-x}Sr_xNiO_{4-\delta}$. *Phys. Rev. B* **2000**, *61*, 3739−3744.
(32) Liu, Z.; Wang, X.; Ye, X.; Shen, X.; Bian, Y.; Ding, W.; Agrestini, S.; Liao, S.-C.; Lin, H.-J.; Chen, C.-T.; et al. Observation of A-site antiferromagnetic and B-site ferrimagnetic orderings in the quadruple perovskite oxide $CaCu_3Co_2Re_2O_{12}$. *Phys. Rev. B* **2021**, *103*, No. 014414.
(33) Long, Y.; Saito, T.; Mizumaki, M.; Agui, A.; Shimakawa, Y. Various valence states of square-coordinated Mn in A-site-ordered perovskites. *J. Am. Chem. Soc.* **2009**, *131*, 16244−16247.
(34) Agrestini, S.; Chen, K.; Kuo, C.-Y.; Zhao, L.; Lin, H.-J.; Chen, C.-T.; Rogalev, A.; Ohresser, P.; Chan, T.-S.; Weng, S.-C.; et al. Nature of the magnetism of iridium in the double perovskite Sr_2CoIrO_6. *Phys. Rev. B* **2019**, *100*, No. 014443.
(35) Feng, H. L.; Chen, J.; Hu, Z.; Wang, X.; Reehuis, M.; Adler, P.; Hoser, A.; Wu, M.-X.; Agrestini, S.; Vasili, H. B.; et al. From antiferromagnetism to high-T_C weak ferromagnetism manipulated by atomic rearrangement in $Ba_3NiOs_2O_9$. *Phys. Rev. Mater.* **2020**, *4*, No. 064420.
(36) Thole, B. T.; Carra, P.; Sette, F.; van der Laan, G. X-ray circular dichroism as a probe of orbital magnetization. *Phys. Rev. Lett.* **1992**, *68*, 1943−1946.
(37) Carra, P.; Thole, B. T.; Altarelli, M.; Wang, X. X-ray circular dichroism and local magnetic fields. *Phys. Rev. Lett.* **1993**, *70*, 694−697.
(38) Saha-Dasgupta, T. Double perovskites with 3d and 4d/5d transition metals: compounds with promise. *Mater. Res. Express* **2020**, *7*, No. 014003.
(39) Chen, W.-t.; Mizumaki, M.; Seki, H.; Senn, M. S.; Saito, T.; Kan, D.; Attfield, J. P.; Shimakawa, Y. A half-metallic A- and B-site-ordered quadruple perovskite oxide $CaCu_3Fe_2Re_2O_{12}$ with large magnetization and a high transition temperature. *Nat. Commun.* **2014**, *5*, 3909.

(40) Deng, H.; Liu, M.; Dai, J.; Hu, Z.; Kuo, C.; Yin, Y.; Yang, J.; Wang, X.; Zhao, Q.; Xu, Y.; et al. Strong enhancement of spin ordering by A-site magnetic ions in the ferrimagnet $CaCu_3Fe_2Os_2O_{12}$. *Phys. Rev. B* **2016**, *94*, No. 024414.
(41) Wang, X.; Liu, Z.; Deng, H.; Agrestini, S.; Chen, K.; Lee, J.-F.; Lin, H.-J.; Chen, C.-T.; Choueikani, F.; Ohresser, P.; et al. Comparative study on the magnetic and transport properties of B-site ordered and disordered $CaCu_3Fe_2Os_2O_{12}$. *Inorg. Chem.* **2022**, *61*, 16929−16935.
(42) Wang, X.; Hu, Z.; Agrestini, S.; Herrero-Martín, J.; Valvidares, M.; Sankar, R.; Chou, F.-C.; Chu, Y.-H.; Tanaka, A.; Tjeng, L. H.; Pellegrin, E. Evidence for largest room temperature magnetic signal from Co^{2+} in antiphase-free & fully inverted $CoFe_2O_4$ in multiferroic-ferrimagnetic $BiFeO_3$-$CoFe_2O_4$ nanopillar thin films. *J. Magn. Magn. Mater.* **2021**, *530*, No. 167940.
(43) Liu, Z.; Zhang, S.; Wang, X.; Ye, X.; Qin, S.; Shen, X.; Lu, D.; Dai, J.; Cao, Y.; Chen, K.; et al. Realization of a half metal with a record-high Curie temperature in perovskite oxides. *Adv. Mater.* **2022**, *34*, No. 2200626.
(44) Tanaka, A.; Jo, T. Resonant 3*d*, 3*p* and 3*s* photoemission in transition metal oxides predicted at 2*p* threshold. *J. Phys. Soc. Jpn.* **1994**, *63*, 2788−2807.
(45) Sahu, R. K.; Hu, Z.; Rao, M. L.; Manoharan, S. S.; Schmidt, T.; Richter, B.; Knupfer, M.; Golden, M.; Fink, J.; Schneider, C. M. X-ray absorption spectra at the Ru and Mn $L_{2,3}$ edges and long-range ferromagnetism in $SrRu_{1-x}Mn_xO_3$ solid solutions ($0 \leq x \leq 0.5$). *Phys. Rev. B* **2002**, *66*, No. 144415.
(46) Burnus, T.; Hu, Z.; Haverkort, M. W.; Cezar, J. C.; Flahaut, D.; Hardy, V.; Maignan, A.; Brookes, N. B.; Tanaka, A.; Hsieh, H. H.; et al. Valence, spin, and orbital state of Co ions in one-dimensional $Ca_3Co_2O_6$: An x-ray absorption and magnetic circular dichroism study. *Phys. Rev. B* **2006**, *74*, No. 245111.
(47) Parameters used in cluster calculations (eV). For Mn^{2+}: U_{dd} = 7.0, U_{cd} = 8.0, Δ = 6.5, H_{ex} = -8.52×10^{-4}. Considering the low symmetry of the MnO_8 polyhedron, the crystal field was obtained from the Madelung potential and the hybridization was obtained from Harrison's prescription. For Co^{2+} (O_h): U_{dd} = 6.5, U_{cd} = 8.2, Δ = 6.5, $10Dq$ = 0.45, V(e) = 1.92, V(t_{2g}) = 1.02, H_{ex} = $-$ 8.30 × 10^{-4}. For Re^{6+} (O_h): U_{dd} = 1.0, U_{cd} = 3.0, Δ = $-$ 2.0, $10Dq$ = 4.6, V(e) = 3.81, V(t_{2g}) = 2.03, H_{ex} = $-$ 5.80 × 10^{-5}. Slater integrals were set to 90, 80, and 70% of Hartree-Fock values for Mn^{2+}, Co^{2+}, and Re^{6+}, respectively.
(48) Morrow, R.; Mishra, R.; Restrepo, O. D.; Ball, M. R.; Windl, W.; Wurmehl, S.; Stockert, U.; Büchner, B.; Woodward, P. M. Independent ordering of two interpenetrating magnetic sublattices in the double perovskite Sr_2CoOsO_6. *J. Am. Chem. Soc.* **2013**, *135*, 18824−18830.
(49) Toyoda, M.; Yamauchi, K.; Oguchi, T. Ab initio study of magnetic coupling in $CaCu_3B_4O_{12}$ (B = Ti, Ge, Zr, and Sn). *Phys. Rev. B* **2013**, *87*, No. 224430.
(50) Anderson, P. W. Antiferromagntism. *Theory of superexchange interaction. Phys. Rev.* **1950**, *79*, 350.
(51) Goodenough, J. B. Theory of the role of covalence in the perovskite-type manganites [La, *M*(II)]MnO_3. *Phys. Rev.* **1955**, *100*, 564.
(52) Kanamori, J. Superexchange interaction and symmetry properties of electron orbitals. *J. Phys. Chem. Solids* **1959**, *10*, 87.
(53) Guo, J.; Wang, S.; Li, W.; Lu, D.; Ye, X.; Liu, Z.; Qin, S.; Wang, X.; Hu, Z.; Lin, H.-J.; et al. A-site Mn^{2+} tuned magnetism and electrical transport properties in the transition-metal-only perovskite oxide $MnCu_3Mn_4O_{12}$. *Phys. Rev. B* **2022**, *105*, No. 054409.
(54) Pradhan, K.; Sanyal, P.; Saha-Dasgupta, T. Magnetism in cation-ordered multicomponent oxide perovskites. *Chem. Mater.* **2024**, *36*, 3829−3836.

https://doi.org/10.1021/acs.jpcc.4c04491
J. Phys. Chem. C 2024, 128, 15668−15675